CHAPTER 141

FORCES ON A SPHERE UNDER LINEAR PROGRESSIVE WAVES

Scott A. Jenkins and Douglas L. Inman
Scripps Institution of Oceanography, University of California
La Jolla, California 92093

ABSTRACT

The rms horizontal forces which result from the action of a linear, deep and intermediate water, laboratory scale waves were measured on submerged spheres removed several diameters from the free surface. The study focuses on unseparated flows encountered at small values of (d_0/D), where d_0 is the orbital diameter and D is the sphere diameter. Under these conditions, a steady streaming around the vertical equator of the sphere was observed, giving rise to a circulation in the sense of rotation of the orbital motion. This phenomena was found to diminish the resultant of the wave pressure on the sphere predicted by potential theory. In approaching the onset of separation, the drag coefficients were found to compare in size with those reported for similar motions in steady unidirectional flow.

INTRODUCTION

Much of the experimental work addressing the problem of wave induced forces on submerged circular bodies have used in-line oscillatory flows; where the motion is simply back-and-forth and $w_\infty/u_\infty = 0$ (as in Keulegan and Carpenter, 1956; Seymour, 1974; and Sarpkaya, 1975). While the conditions of these experiments may approximate the flows encountered under shallow water waves, it is not clear whether these data are appropriate to the design of offshore structures encountering intermediate or deep water waves, under which the motion is orbital and $w_\infty/u_\infty = \tanh k(z + h)$, after linear theory.

Previous experiments in which progressive waves have been used to create oscillatory motion (O'Brien and Morison, 1952; and Grace and Casciano, 1969) have involved separated local flow over spheres usually in close proximity to the bottom. Under waves, unseparated motions are a consequence of vorticity being confined by small particle orbits to the immediate neighborhood of the body, when $d_0/D < 1$, despite the fact that large Reynolds numbers may prevail. The unseparated flow regime has not yet received thorough experimental scrutiny, particularly for orbital motion, and this lack of information is critical in the design of submerged structures whose cross-sectional dimension may exceed the amplitude of the water motion.

The following study explores these areas by providing measurements of the wave loads on a smooth sphere which result from the orbital motions under linear, intermediate and deep water laboratory scale surface waves, when the local flow is unseparated.

Force Estimates

Instead of pursuing estimates of the wave force time history, we seek estimates of rms values of the force from Morison's equation as useful "engineering numbers". In this way, the time invariant coefficients of the drag and

inertial terms are physically plausable as time averaged values. With these coefficients, only a spectrum of the free surface is required to establish the relative size of horizontal rms values of the drag to the inertia forces at a given frequency by the following

$$\frac{F_f}{F_m} = \frac{c_f \rho A_0 (u_\infty |u_\infty|)_{rms}}{c_m \rho V_0 (\dot{u}_\infty)_{rms}} = \frac{3\sqrt{3}}{8} \frac{c_f}{c_m} \left(\frac{d_{0\ rms}}{D} \right)$$

where $\quad d_{0\ rms} = H_{rms} \dfrac{\cosh k(h - b)}{\sinh kh}$

The anticipated Strouhal dependence arising from a ratio of convective to unsteady inertial terms is equivalent for linear waves to a ratio of the size of the undisturbed particle orbits to the body, (d_0/D). Thus, under the condition for which unseparated motions are found, namely $(d_0/D < 1)$, the inertia force appears as the larger component of the wave load.

The inertia force can be estimated with a scattering description under the hypothesis of potential flow for a sphere submerged at least one diameter, D, under linear deep water waves. The inertia force is the resultant of the local wave pressure,

$$F_{mi} = \iint \rho \frac{\partial \Phi}{\partial t} n_i dS$$

where three independent wave profiles combine linearly to give Φ on the surface of the sphere. The first of these is the undisturbed incident wave, ϕ_∞. Thus, if $kD \ll 1$, the undisturbed incident wave acts to accelerate the sphere into orbital motion like an equivalent volume of water, and contributes $\rho V_0 \dot{u}_\infty$ to the inertia force, giving a time independent value of unity for the inertia coefficient. However, the undisturbed incident wave cannot alone meet the condition of no flow through the sphere, and so a disturbance, ϕ_s, due to the presence of the sphere is added. This disturbance or scattered wave is determined so that the normal velocity over the surface of the sphere is zero

$$\frac{\partial}{\partial r} (\phi_\infty + \phi_s) = 0 \quad \text{at} \quad r = D/2$$

There is an additional pattern of disturbances, Froude waves, as a consequence of the proximity of the sphere to the free surface. However, if the sphere is at rest, and, if the depth of submergence is taken to be D, where $d_0/D < 1$, then the Froude number is $O(\epsilon d_0/D)^{\frac{1}{2}}$ and it may be verified that any contribution to the force by Froude waves is altogether negligable after first order linear theory due to Havelock (1952) and after complete second order theory due to Kim (1969).

Expanding the spacially dependent parts of the incident and scattered waves into a series of tesseral spherical harmonics, Lamb (1932, art 86 and 106) as,

$$\exp(kz + ikx) = \exp(kr \sin\theta\sin\omega + ikr\cos\theta) = \sum_n \sum_s A_n^s P_n^s(\cos\theta) \cos s\omega$$

yields a scattering formulation which does not rely on the plane wave approximation as for acoustic scattering, or for scattering of surface waves by a vertical cylinder. The orthogonality on a spherical surface of the set of surface harmonics,

$$P_n^s(\cos\theta) \cos s\omega$$

taken with the condition of no flow through the sphere and the radiation condition,

$$\Phi = \phi_\infty + \phi_\infty(D/2x)^{\frac{1}{2}} \quad (|\Phi_r = D/2|/|\phi_\infty|)$$

as $x \to \infty$ yields the coefficients, A_n^s, for the incident and scattered waves. These have been evaluated in Havelock (1954) and specify the pressure over the surface of the sphere resulting in the following expressions for the horizontal and vertical components of the inertia force

$$F_{m_x} = \frac{1}{4} \rho g D^2 (2\pi)^{3/2} \frac{H}{2} e^{-kb} (1 + 1/2)(kD/2)^{-1/2} J_{3/2}(kD/2) \sin(-\sigma t)$$

$$F_{m_z} = \frac{1}{4} \rho g D^2 (2\pi)^{3/2} \frac{H}{2} e^{-kb} (1 + 1/2)(kD/2)^{-1/2} J_{3/2}(kD/2) \cos(-\sigma t)$$

Normalizing the amplitudes of the horizontal and vertical components by the amplitudes of $\rho V_0 \dot{u}_\infty$ and $\rho V_0 \dot{w}_\infty$ respectively gives the following time independent inertia coefficient for both components

$$c_m = \frac{3}{2} (1 + c_a)(kD)^{-3/2} J_{3/2}(kD/2)$$

where $c_a = 1/2$ and is plotted in Figure 1. When the sphere becomes small in relation to the wave length, c_m is found to converge to 1.5, the value for a sphere in an unbounded uniformly accelerating fluid, and thereby supporting assumptions made in this regard in the early work of O'Brien and Morison (1952). Furthermore the horizontal and vertical components are found to lead the wave profile in time by constant phase angles of $\pi/2$ and π respectively. However, once $kD/2 \gg 1$, c_m becomes small and oscillating as

$$c_m = \frac{g}{4} \sqrt{\frac{2}{\pi}} (kD/2)^{-2} \cos(kD/2 - \pi)$$

for $kD/2 \gg 1$. As a result, the phase of the inertia force relative to the incident wave profile varies rapidly with wave number, since the incident wave is now leaking around a very large obstacle. The lack of a dependence in c_m on the depth of submergence is a consequence of neglecting the effects of Froude waves by limiting the analysis to the case where $b > D$.

If the sphere is subjected to shallow water waves, then $w_\infty/u_\infty \tilde{=} 0$ and the acoustic plane wave approximation appears admissible. Scattering of plane waves by a spherical obstacle is treated in Lamb (1932, art no 296) and results in an inertia coefficient which converges in the small body limit, $kD/2 \ll 1$, to 1.5 as

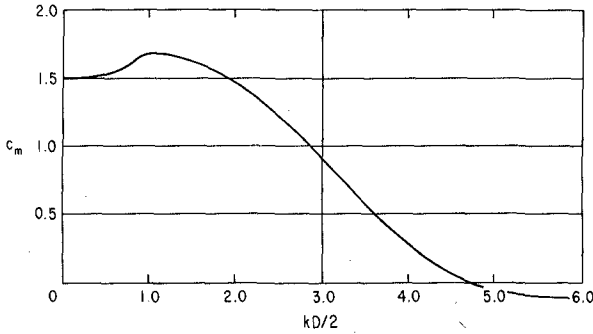$$c_m = 1 + \frac{2 + (kD/2)^2}{4 + (kD/2)^4}$$

Figure 1.   Spherical deep water scattering solution for the inertia coefficient, c_m, after Havelock (1954), where k is the wave number $= 2\pi/$wave length; D is the sphere diameter.

Experiment

The horizontal component of the wave load was measured for polished spheres of 10 cm and 20 cm diameters subjected individually to discrete frequency waves of 0.2, 0.4, 0.6 and 0.75 Hz and heights of 5, 10, 15, and 20 cm, for a total of 32 separate experiments in the 2.5 meter wide wind and wave channel in the Scripps Institution Hydraulics Laboratory. The spheres were situated at mid-depth in 154 cm of water. This choice of experimental parameters limited the investigation to be consistent with the previously stated assumptions and regimes of interest by insuring negligible Froude wave effects $(0.012 < F_r < 0.11)$, orbital motion, $(0.24 < w_\infty/u_\infty < 0.93)$, and thorough coverage of the regime of small amplitude motion up to the onset of separation $(0.053 < d_0/D < 3.5)$. The study however was limited to examination of the small body limit $(0.017 < kD/2 < 0.216)$ due to the problem of cross channel waves when attempting to generate waves which are shorter than the sphere diameter in a channel which must necessarily be significantly wider than D.

The measured horizontal force, F, was resolved in the frequency domain into the drag and inertia components of the Morison estimator, $\hat{F}$, by a harmonic analysis technique adapted from Seymour (1974), involving minimizing the mean squared error in $<(F - \hat{F})^2>$ where

$$\hat{F} = c_1 u_\infty |u_\infty| + c_2 \dot{u}_\infty$$

$$c_1 = \rho c_f A_0$$

$$c_2 = \rho c_m V_0$$

$$<(F - \hat{F})^2> = <F^2> + c_1^2 <(u_\infty|u_\infty|)^2> + 2c_1 c_2 <u_\infty|u_\infty|\dot{u}_\infty> + c_2^2 <\dot{u}_\infty^2> - 2c_1 <Fu_\infty|u_\infty|>$$

$$- 2c_2 <F\dot{u}_\infty>$$

If the incident waves are linear, then

$$< u_\infty |u_\infty| \dot{u}_\infty > = 0$$

Expressing the covariance and variance in terms of the cospectral and spectral estimates, $<xy> = C_{x,y}$ and $<x^2> = S_x$, and taking $\partial/\partial c_i <(F - F)^2> = 0$, solving for c_1 and c_2 gives

$$c_f = \frac{8}{\rho \pi D^2} \frac{C_{F, u_\infty |u_\infty|}}{S_{u_\infty |u_\infty|}}$$

and

$$c_m = \frac{6}{\rho \pi 0^3} \frac{C_{F, \dot{u}_\infty}}{S_{\dot{u}_\infty}} = \frac{6}{\rho \pi 0^3} \frac{C_{F, x}}{\sigma^2 S_x}$$

To arrive at c_f and c_m using this scheme each individual experiment was repeated four times during which time histories of horizontal force and free surface elevation were sampled and stored on magnetic tape using an IBM 1130 computer system. As much frequency resolution as possible was desirable. However, a limit of 2048 samples per record was imposed by the 1130 system and a need for as many samples per wave cycle as possible to adequately define the wave profiles led to the compromise of sampling at 20 Hz to allow each run a duration of 102.4 sec and a frequency resolution of 0.0097 Hz. After transforming these time series using Fast Fourier transform routines, the Fourier coefficients for the horizontal particle position required to construct S_x and $C_{F,x}$ were obtained from those of the free surface through phase shifting $\pi/2$ by reversing the cosine and sine coefficients, changing the sign of the cosine coefficient and then multiplying by

$$\frac{\cosh k(h - b)}{\sinh kh}$$

after linear theory. The Fourier coefficients for $u_\infty |u_\infty|$ were obtained by taking derivatives (slopes) of the free surface time series, squaring, and then transforming to the frequency domain. The resulting Fourier pairs representing the square of the vertical velocity at the free surface were then phase shifted by $\pi/2$ as before and attenuated to the depth of submergence as;

$$\left(\frac{\cosh k(h - b)}{\sinh kh} \right)^2$$

The drag and inertia coefficients realized in this way from the principle frequency band of each run were then averaged among the set of quadruplicate runs comprising each separate experiment.

Because this method relies heavily on the average time dependence of u_∞ being zero, care was taken to minimize seiching and reflection in the wave channel by submerging a tethered floating breakwater at the beach end. In addition, only wave forms of small steepness were used, with $0.008 < \epsilon < 0.22$. To minimize generation of a free second harmonic due to the paddle motion, the

paddle throw was adjusted to a flapper mode for the deep water waves and to a
semi-piston/flapper mode for the intermediate water waves.

Results of the Force Experiment

An example of the grouped spectra of horizontal force and the free
surface when unseparated local flow persists is found in Figure 2, using a 10
cm sphere under a 0.75 Hz, 20 cm wave. The linear character of the incident
waves is evidenced by the negligible energy appearing at harmonics above the
driving frequency. The second harmonic in the force spectra is two orders of
magnitude below the peak at the driving frequency where a phase difference of
$\pi/2$ with the free surface is seen, indicating the predominance of the inertia
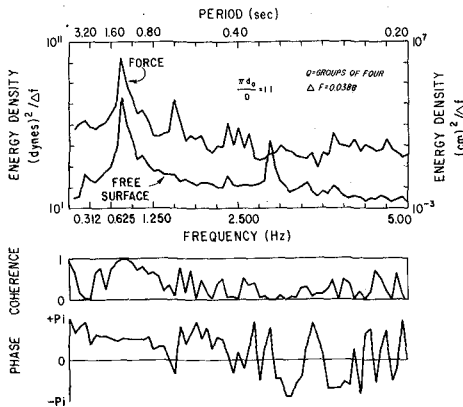force.

Figure 2. Grouped spectra of the free surface and horizontal force for unsep-
arated orbital motion.

Flow visualization using dye injection from three parts embedded in
the spheres at 90° increments around the horizontal equator demonstrated as in
Figures 3-5 that the local flow is both laminar and unseparated for $\pi d_0/D < 3.2$.
Surprisingly, the dye streaks from the forward and aft ports produced by several
cycles of motion show in Figures 3 and 4 a steady streaming close to the sur-
face of the sphere, superposed on the local particle motion, causing a circula-
tion around the vertical equator in the sense of rotation of the orbital motion,
despite the linear character of the incident waves. Similarly, dye released
from the side port in Figure 5 circulates in multiple cycles as laminar stream-
ing around latitudinal belts in the vertical plane. As $\pi d_0/D$ exceeded 3.2
and the orbits became increasingly flattened the circulation became turbulent
as seen in Figure 6, in response to adverse pressure gradients imposed by the
wave field prior to each flow reversal. By $\pi d_0/D = 7$ the onset of separation
was observed when portions of the dye plume would break away from the sphere
at the moment of reversal of the local flow, disrupting the turbulent circula-
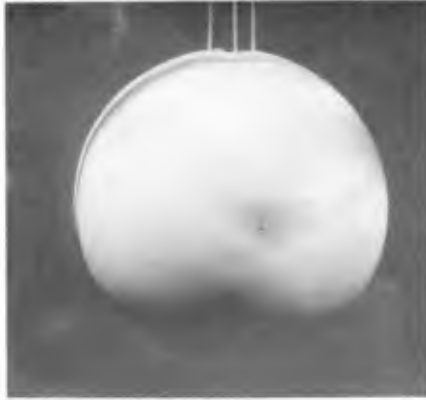tion.

Figure 3. Dye streak produced by two cycles of motion showing circulation
proceeding over the top of the sphere at $\pi d_0/D = 3.2$. Waves progressing
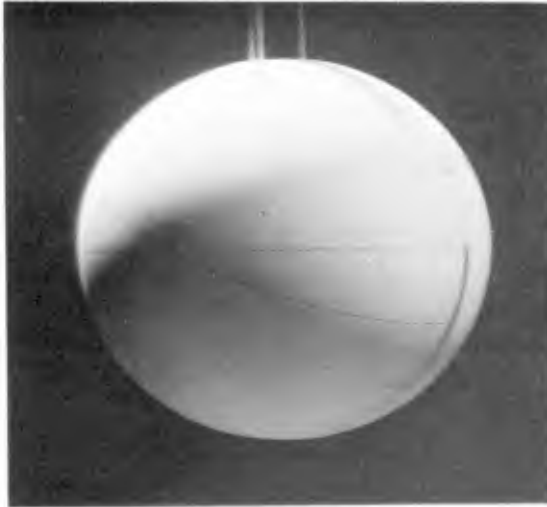from left to right.

Figure 4. Circulation carries dye 6 cm in two cycles from rear port towards
the underside of the sphere at $\pi d_0/D = 0.32$. Waves progressing from left
to right.

Figure 5. Dye spreading in a spiral from the side port towards the vertical equator at $\pi d_0/D = 1.1$. Waves progressing from left to right.
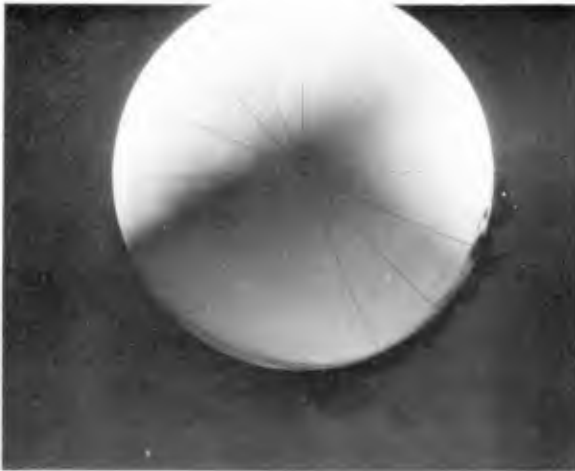

Figure 6. Turbulent circulation carrying dye plume from the rear port around the bottom of the sphere for $\pi d_0/D = 4.0$.

The drag coefficients measured in this investigation were found to vary system-atically with the Keulegan-Carpenter form of the Strouhal number as shown in Figure 7. For $\pi d_0/D < 3.2$, the sizes of the drag coefficients were typical of those for unseparated steady unidirectional flow around a sphere at low Reynolds number ($0.6 < R < 25$). In the range $3.2 < \pi d_0/D < 7$ where turbu-lent circulation was observed, c_f was found to be comparable to values measured for steady unidirectional flow when closed streamlines behind a sep-aration bubble are found for $25 < R < 150$. Indeed the turbulent circulation may evolve as a separation bubble formed near flow reversal and then convected around the sphere under the influence of orbital motion. When $\pi d_0/D > 9$ and the onset of separation is clearly developed the values of c_f measured here are found to compare in size with those reported for a sphere in steady trans-lation with fully separated flow and open-ended streamlines at about $R = 10^4$. The range of Reynolds numbers covered in this study was from 0.5×10^4 to 4×10^4, based on the amplitude of the horizontal velocity component.
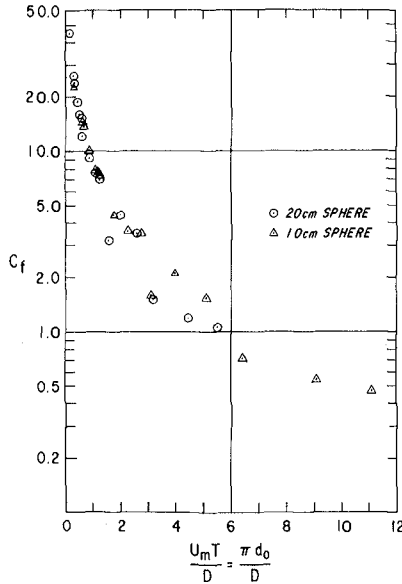

Figure 7. Measured drag coefficients, c_f, against the inverse of the Strouhal number, $u_m T/D = \pi d_0/D$, where u_m is the maximum horizontal particle velocity in the undisturbed wave; T is the wave period and d_0 is the orbital diameter.

The measured inertia coefficients, c_m, Figure 8, defy explanation in terms of the results of the scattering problem. To find the values all less than unity is particularly surprising, and, since the sphere is so small in relation to the incident wave length, the pressure of the undisturbed wave

alone should result in an inertia coefficient of unity. Any scattering of the incident wave would add to this. The circulation, which could not be generated in the absence of viscosity for simple harmonic motions appears to be the only physical explanation for these values.
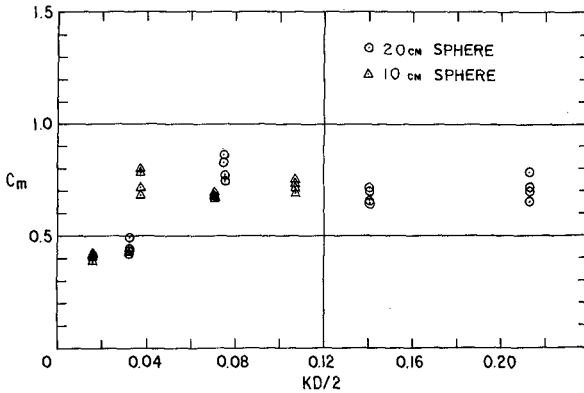

Figure 8. Measured inertia coefficients, c_m, against $kD/2$.

Circulation Streaming

Nonlinear free-surface effects as considered in Kim (1969) for a submerged sphere do not appear a likely mechanism for generating the circulation observed in this study due to the remoteness of the sphere from the free surface $(3.8\ D <\ b < 7.7\ D)$ and the small size of the sphere with respect to the incident wave length. Furthermore, the streaming appears most intense near the surface of the sphere. Therefore, the boundary layer does seem a likely mechanism.

Schlichting (1966) has treated the problem of steady streaming as developed by a circular cylinder executing small amplitude oscillations in still water. Photographic evidence of similar streaming near a cylinder due to acoustic waves in air may be found in a paper by Holtsmark, et al (1954). However, the streaming developed by these in-line oscillatory flows does not result in a net circulation because the streaming flows away from the cylinder along the axis in line with the oscillations, and towards it at locations transverse to these oscillations.

Streaming over a flat bottom under the orbital motion of progressive waves, "bottom wind", has been treated in Longuet-Higgins (1953) and shown to be a consequence of the retarding influence of the boundary layer being greater for that portion of the orbit in closest proximity to the wall. Consider, then, in Figure 9, the solid path lines of deformed, closed orbits in the vicinity of a submerged sphere under linear inviscid, irrotational waves when $kD/2 << 1$. There is negligible decay in the amplitude of the motion vertically over one sphere diameter, and no net time independent motions result. But if viscosity and the formation of boundary layers is allowed in the model,

then the orbits can no longer remain closed and a "bottom wind" results around the sphere to give rise to a time independent circulation in the sense of rotation of the orbital motion. Considerably more vigorous streaming may be realized around a sphere than over a flat bottom, because in diffracting around the sphere the local velocities and orbital diameters are increased relative to those in the undisturbed field, with diffraction velocities approaching $3/2\ u_\infty$ for $kD/2 \ll 1$.
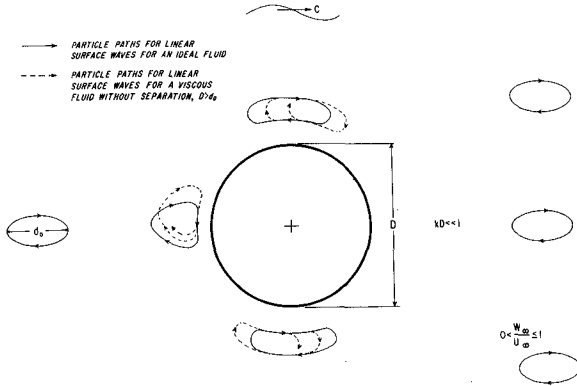

Figure 9. "Bottom wind" around a sphere as a mechanism for circulation streaming.

        The streaming velocities around the vertical equator were estimated for each wave condition in the force experiments by measuring the progress of the leading edge of a dye streak for an integral number of wave cycles. The dye was released from the rear port from where it proceeded around the bottom of the sphere and was thus not perturbed by the small diameter sting used to support the sphere from the surface. The circumferential streaming velocity $<u_\theta>$, was found to be almost linear with $(d_0 w_\infty/\pi D)$ as shown in Figure 10. At large values of $(d_0 w_\infty/\pi D)$ the streaming was more difficult to measure due to turbulence, but tended to decay and then quickly degenerate with the onset of separation. These results demonstrate that for a given wave height the circulation will be most intense for a deep water wave and diminishes as the wave becomes shallow water in character, and cease altogether once the motion is merely back-and-forth, assuming separation has not yet set in.

        With such a circulation added to the diffracting velocity field, the action of fluid inertia must result in a force historically termed as lift, F_ℓ, which acts normally to the instantaneous far field velocity and will therefore rotate through 2π in a wave cycle. Because the circulation is in the sense of rotation of the orbital motion, and because the phase of the inertia force lags the wave profile in space by a constant $\pi/2$ when $kD/2 \ll 1$, the lift opposes the inertia force at any given wave phase as illustrated schematically in Figure 11. Because the streaming is generated at the top of the ac boundary layer, $O(\nu/\sigma)^{\frac{1}{2}}$, it is assumed that the Kutta-Joukowski theorem is appropriate to estimate rms values of the horizontal

component of lift. This presuposes that the streaming velocity $<u_\theta>$, decays as $(1/r)$ and this has not yet been verified. In addition, the circulation distribution from the vertical equator to the sides transverse to the waves must be specified. The expanding spiral shaped dye streak issued from the side port in Figure 5 show that the streaming diminishes towards the sides of the sphere. If an assumption of solid body rotation is applied to the region within the vortex tube which results from the circulation around the vertical equator, then the streaming velocity $<u_\theta>$, decays from the vertical equator to zero at the sides as $\cos\omega$. The rms value of the horizontal component of lift can then be estimated from only knowing the streaming around the vertical equator, $<u_\theta>$ and from $w_{\infty rms}$ by

$$F_{\ell_{rms}} = \frac{2}{3} \rho \pi D^2 <u_\theta> (w_\infty)_{rms}$$

where the vertical motion gives rise to the horizontal component of lift. Because the horizontal component of F_ℓ opposes the horizontal component of the inertia force, its rms values can be normalized by $\rho V_0 (\dot{u}_\infty)_{rms}$ and then added to the measured values of, c_m in Figure 6, thereby subtracting the viscous effects due to circulation to give apparent inviscid values for the inertia coefficient plotted in Figure 12. Many of these values are comparable in size with the expectations of the scattering solution. However, due to the approximations in computing $F_{\ell_{rms}}$ these are presented here only to illustrate that the circulation can augment the inertia force at least to an extent that can account for the very small values of c_m measured in this study.
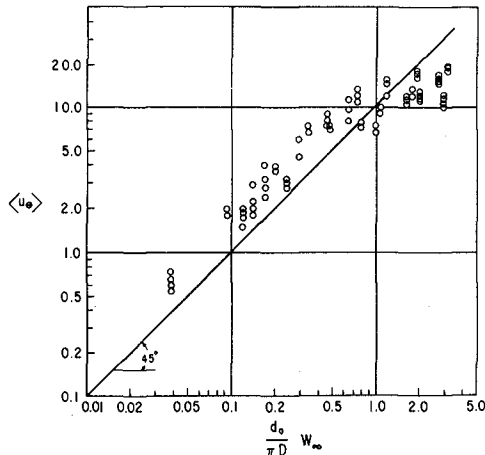

Figure 10. Streaming velocities $<u_\theta>$, measured around the vertical equator of the sphere against $(d_0 w_\infty/\pi D)$ where w_∞ is the amplitude of the vertical particle velocity in the undisturbed wave. Velocities are expressed in units of cm/sec.
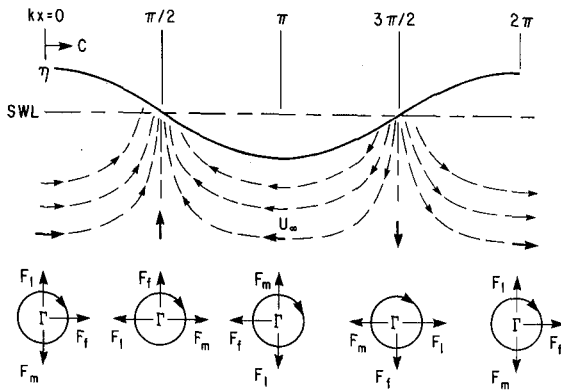
Figure 11. Phase relationships between drag, F_f, the inertia force, F_m, and lift, F_ℓ, relative to the wave profile when a circulation, Γ, in the sense of the orbital motion is present.
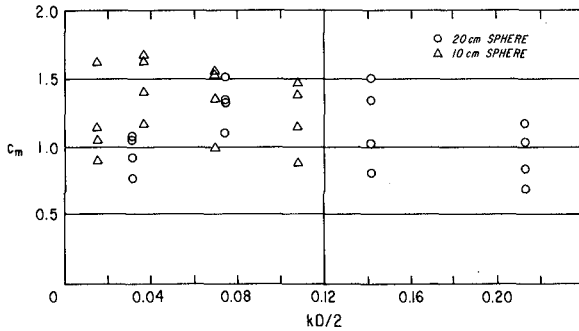

Figure 12. Apparent inviscid inertia coefficients, c_m, obtained by correcting measured values of c_m for the horizontal component of lift.

Conclusions

Even when the gross viscous effects associated with separation are avoided, the smaller viscous effects which prevail in unseparated orbital motion and give rise to circulation streaming are sufficiently important to render potential theory as a rather poor description of the problem of forces induced by linear progressive waves. Because the circulation phenomena cannot be accounted for by in-line oscillatory flow, such studies are inappropriate to the design of circular members which exceed the amplitudes of the motions under deep and intermediate water waves.

Symbols

A_n^s	solid harmonic coefficient
A_o	frontal area of a sphere = $\pi D^2/4$
b	depth of submergence
c_a	added mass coefficient
c_f	drag coefficient = constant in the time domain
c_m	inertia coefficient = constant in the time domain
C_{xy}	cospectral estimate
D	sphere diameter
d_o	orbital diameter in the undisturbed wave
F_f	drag force
F_ℓ	lift force
F_m	inertia force
F_r	Froude number = $u_\infty/\sqrt{gb}$
$\hat{F}$	Morison estimator
g	acceleration of gravity
H	wave height
h	water depth
$J_{n + 1/2}$	Bessel function of the first kind and half odd integral order with argument = $kD/2$
k	wave number
n_i	direction cosine

p_n^s Legendre function of order s and degree n with argument $= \cos\theta$

r radial coordinate

R Reynolds number

s order

S spherical surface area

S_x spectral estimate

t time variable

V_o volume of the sphere $= \pi D^3/6$

u_∞ horizontal particle velocity in the undisturbed wave $= \partial\phi_\infty/\partial x$ at the depth of submergence of the sphere

$\dot{u}_\infty$ horizontal particle acceleration in the undisturbed wave at the depth of submergence of the sphere

u_θ circumferential velocity component

V_o volume of the sphere $= \pi D^3/6$

w_∞ vertical particle velocity in the undisturbed wave, $= \partial\phi_\infty/\partial z$ at the depth of submergence of the sphere

x, y, z Cartesian coordinates with the x-axis in the direction of wave advance, the y-axis transversely, and the z-axis positive upwards

Γ circulation

ε wave steepness $= kH/2$

Φ local velocity potential $= \phi_\infty + \phi_S$

ϕ_∞ velocity potential of the undisturbed incident deep water waves $= (H\sigma/2k)\,\exp(kz)\,\sin(kx - \sigma t)$

ϕ_S velocity potential of the scattered wave

ρ fluid density

σ radian frequency $= 2\pi/$wave period

θ angular coordinate in the xz plane

ω angular coordinate in the xy plane

$|\ |$ absolute value

$<\ >$ time average

References

Grace, R. A. and F. M. Casciano, 1969, "Ocean wave forces on a subsurface sphere", Jour. Waterways and Harbors Div., Proc. Amer. Soc. Civil Eng., WW3, Paper no 6722, p 291-317.

Havelock, T. H., 1952, "The moment on a submerged solid of revolution moving horizontally", Quart. Jour. Mech. Appl. Math., vol 5, p 129-36.

Havelock, T. H., 1954, "The forces on a submerged body moving under waves", Quart. Trans. of Inst. of Naval Arch., January, and in The Collected Papers of Sir Thomas Havelock on Hydrodynamics, ONR/ACR-103, pp 590-96.

Holtsmark, J., I. Johnsen, T. Sikkeland and S. Skavlem, 1954, "Boundary layer flow near a cylindrical obstacle in an oscillating incompressible fluid", Jour. Acoust. Soc. Amer., vol 26, p 102.

Keulegan, G. H. and L. H. Carpenter, 1956, "Forces on cylinders and plates in an oscillating fluid", Nat. Bureau of Standards, Report No 4821, 57 pp.

Kim, W. D., 1969, "Nonlinear free-surface effects on a submerged sphere", Jour. Hydronautics, vol 3, no 1, p 29-37.

Lamb, H., 1932, Hydrodynamics, Cambridge University Press, 738 pp.

Longuet-Higgins, M. S., 1953, "Mass transport in water waves", Phil. Trans. Roy. Soc. London, Series A, no 903, vol 245, p 535-581.

O'Brien, M. P. and J. R. Morison, 1952, "The forces exerted by waves on objects", Trans. Amer. Geophys. Union, vol 33, no 1, p 32-8.

Sarpkaya, T., 1975, "Forces on cylinders and spheres in a sinusoidally oscillating fluid", Jour. Applied Mech., Trans. Amer. Soc. Mech. Eng., vol 42, no 1, p 32-7.

Schlichting, H., 1966, Boundary Layer Theory, McGraw-Hill Inc., New York, 747 pp.

Seymour, R. J., 1974, "Resistance of spheres in oscillatory flows", Ph. D. Dissertation, Scripps Institution of Oceanography, University of California, San Diego, 86 pp.